

Single-frequency linearly polarized *Q*-switched fiber laser based on Nb_2GeTe_4 saturable absorber

Si-Yu Chen(陈思雨), Hai-Qin Deng(邓海芹), Wan-Ru Zhang(张万儒), Yong-Ping Dai(戴永平), Tao Wang(王涛), Qiang Yu(俞强), Can Li(李灿), Man Jiang(姜曼), Rong-Tao Su(粟荣涛), Jian Wu(吴坚), and Pu Zhou(周朴)
Citation: Chin. Phys. B, 2023, 32 (**7**): 074203. DOI: 10.1088/1674-1056/acad6d
Journal homepage: http://cpb.iphy.ac.cn; http://iopscience.iop.org/cpb

What follows is a list of articles you may be interested in

Antimonene-based saturable absorber for a soliton mode-locked and *Q*-switched fiber laser in the 2 μm wavelength region

H Ahmad, B Nizamani, M Z Samion, N Yusoff, and M F Ismail
Chin. Phys. B, 2023, 32 (**6**): 064205. DOI: 10.1088/1674-1056/ac891f

High efficiency of Brillouin scattering behavior in single-mode Ge-As-Se-Te fibers at 2 μm

Yue Fu(付悦), Shi-Xun Dai(戴世勋), Lu-Lu Xu(徐路路), Yao-Jun Fang(方耀俊), Ying-Ying Wang(王莹莹), Kai Jiao(焦凯), and Xun-Si Wang(王训四)
Chin. Phys. B, 2023, 32 (**5**): 054206. DOI: 10.1088/1674-1056/ac9a3a

A kind of multiwavelength erbium-doped fiber laser based on Lyot filter

Zhehai Zhou(周哲海), Jingyi Wu(吴婧仪), Kunlong Min(闵昆龙), Shuang Zhao(赵爽), and Huiyu Li(李慧宇)
Chin. Phys. B, 2023, 32 (**3**): 034205. DOI: 10.1088/1674-1056/ac872b

Impact of amplified spontaneous emission noise on the SRS threshold of high-power fiber amplifiers

Wei Liu(刘伟), Shuai Ren(任帅), Pengfei Ma(马鹏飞), and Pu Zhou(周朴)
Chin. Phys. B, 2023, 32 (**3**): 034202. DOI: 10.1088/1674-1056/ac833e

Real-time observation of soliton pulsation in net normal-dispersion dissipative soliton fiber laser

Xu-De Wang(汪徐德), Xu Geng(耿旭), Jie-Yu Pan(潘婕妤), Meng-Qiu Sun(孙梦秋), Meng-Xiang Lu(陆梦想), Kai-Xin Li(李凯芯), and Su-Wen Li(李素文)
Chin. Phys. B, 2023, 32 (**2**): 024210. DOI: 10.1088/1674-1056/ac76b0

Single-frequency linearly polarized *Q*-switched fiber laser based on Nb_2GeTe_4 saturable absorber

Si-Yu Chen(陈思雨)[1], Hai-Qin Deng(邓海芹)[1], Wan-Ru Zhang(张万儒)[1], Yong-Ping Dai(戴永平)[3], Tao Wang(王涛)[1], Qiang Yu(俞强)[1,3], Can Li(李灿)[1], Man Jiang(姜曼)[1,2], Rong-Tao Su(粟荣涛)[1,2,†], Jian Wu(吴坚)[1,‡], and Pu Zhou(周朴)[1]

[1] *College of Advanced Interdisciplinary Studies, National University of Defense Technology, Changsha* 410073, *China*
[2] *Nanhu Laser Laboratory, National University of Defense Technology, Changsha* 410073, *China*
[3] *CAS Key Laboratory of Nanophotonic Materials and Devices & Key Laboratory of Nanodevices and Applications, i-Lab, Suzhou Institute of Nano-Tech and Nano-Bionics (SINANO), Chinese Academy of Sciences (CAS), Suzhou* 215123, *China*

(Received 16 November 2022; revised manuscript received 9 December 2022; accepted manuscript online 21 December 2022)

We report a single-frequency linearly polarized *Q*-switched fiber laser based on an Nb_2GeTe_4 saturable absorber (SA). The Nb_2GeTe_4 SA triggers passive *Q*-switching of the laser, and an un-pumped Yb-doped fiber together with a 0.08-nm-bandwidth polarization-maintaining fiber Bragg grating (FBG) acts as an ultra-narrow bandwidth filter to realize single-longitudinal-mode (SLM) oscillation. The devices used in the laser are all kept polarized, so as to ensure linearly polarized laser output. Stable SLM linearly polarized *Q*-switching operation at 1064.6 nm is successfully achieved, producing a laser with a shortest pulse width of 1.36 μs, a linewidth of 28.4 MHz, a repetition rate of 28.3 kHz–95.9 kHz, and a polarization extinction ratio of about 30 dB. It is believed that the single-frequency linearly polarized pulsed fiber laser studied in this paper has great application value in gravitational wave detection, beam combining, nonlinear frequency conversion, and other fields.

Keywords: fiber laser, saturable absorber, single-longitudinal-mode, pulsed laser

PACS: 42.55.–f, 42.55.Wd, 42.60.Gd, 42.65.Pc **DOI:** 10.1088/1674-1056/acad6d

1. Introduction

The *Q*-switched fiber lasers are widely used in applications such as optical fiber sensing, material processing, and optical communications due to their virtues of narrow pulse width, high peak power, and high pulse energy.[1–4] Currently, most of *Q*-switched fiber lasers operate in the multi-longitudinal-mode (MLM) regime. However, compared with MLM *Q*-switched fiber lasers, SLM *Q*-switched fiber lasers with ultra-narrow linewidth and long coherence length are very preferable in the fields of beam combining, nonlinear frequency conversion, and lidar.[5–9]

The SLM laser can be achieved by using Fabry–Perot cavity, saturated absorber (SA), and stimulated Brillouin scattering.[10–12] Recently, the use of SA combined with FBG to generate SLM laser has been widely studied.[13–15] *Q*-switching operation of SLM fiber lasers can be achieved through either active approach or passive approach.[16–18] Active *Q*-switching usually requires an additional electro–optic or acoustic-optic modulator in the laser cavity. Li *et al*. achieved a mode-hopping-free SLM pulsed laser output by using an electro–optic modulator as an active *Q*-switched component and injecting the single-frequency seed laser into the ring cavity.[19] Wang *et al*. obtained the SLM pulsed laser by using an acoustic–optic modulator as the active *Q*-switcher and injecting SLM seed light into the cavity.[20] Zhao *et al*. utilized a fiber stretcher to introduce stress-induced birefringence modulation, combined a distributed Bragg reflector resonant cavity with polarizations loss anisotropy, and realized an SLM actively *Q*-switched fiber laser with uniform Gaussian-shape pulses output.[21] Active *Q*-switched fiber lasers have the advantages of stable performance, strong practicability, and adjustable repetition rate.[22] However, it will inevitably increase the complexity and cost of the system due to the additional devices in the cavity. In recent years, passive *Q*-switching has been vigorously developed due to the virtues of compact structure, simplicity, and flexibility in design.[23–25] As shown in earlier reports,[16,17] the researchers realized the SLM pulsed laser output at 1.5 μm and 2 μm based on a semiconductor saturable absorber mirror (SESAM). The SESAM provides several benefits, such as being compact, robust and free from optical alignment, and portable.[26–28] As an alternative to SESAM, the other saturable absorbers such as two-dimensional (2D) materials, specifically, topological insulators (TIs), 2D ternary tellurides, have attracted a lot of attentions due to the virtues of low cost and ideal nonlinear optical properties.[29–31] Li *et al*. added a few-layer Bi_2Se_3 (which is a kind of TIs) saturable absorber in the ring cavity to achieve passive *Q*-switching, and used an un-pumped erbium-doped fiber together with a 0.06-nm-bandwidth fiber Bragg grating

†Corresponding author. E-mail: surongtao@126.com
‡Corresponding author. E-mail: wujian15203@163.com

© 2023 Chinese Physical Society and IOP Publishing Ltd

as an ultra-narrow filter to obtain single-frequency pulsed laser with a central wavelength of 1550 nm and a pulse duration of 2.54 μs.[25] Compared with the Bi_2Se_3, the Nb_2GeTe_4, which is a kind of 2D ternary telluride, is more preferable for short pulse generation due to its lower saturation intensity and higher modulation depth.[25,32]

The laser with the linearly-polarized property possesses unique advantages in the fields of gravitational wave detection, beam combining, and nonlinear frequency conversion, while none of the above studies seem to give the linearly-polarized property. In this work, we demonstrate a single-frequency linearly polarized passively Q-switched fiber laser, in which all the devices are kept polarized. The un-pumped Yb-doped fiber (YDF) combined with a fiber Bragg grating is used to achieve the SLM oscillation. The passive Q-switching is performed by using the saturable absorption effect of the Nb_2GeTe_4 SA. We therefore obtain the single-frequency linearly polarized pulsed laser at 1064.6 nm. And the laser has a pulse width in a range of of 1.36 μs–1.84 μs, a repetition rate ranging from 32.6 kHz to 95.9 kHz, a linewidth of 28.4 MHz, and a polarization extinction ratio of about 30 dB. The maximum average output power is 4.34 mW, and the maximum single-pulse energy is calculated to be 51.8 nJ. This type of single-frequency pulsed fiber laser has extensive application prospect in nonlinear frequency conversion, lidar systems, and gravitational wave detection.

2. Experimental setup

The experimental setup of single-frequency linearly polarized Q-switched fiber laser based on an Nb_2GeTe_4 SA is shown in Fig. 1. A 976-nm laser diode was used as a pump source to couple the pump light into the ring cavity through a 976 nm/1064 nm polarization-maintaining wavelength division multiplexer (PM-WDM). The gain medium was a section of 1-m polarization-maintaining Yb-doped fiber (PM-YDF1) with a core/cladding diameter of 6 nm/125 μm. A polarization-maintaining circulator (PM-CIR) was used to ensure unidirectional laser operation in the cavity. A mechanical exfoliation process was used to create the high-quality Nb_2GeTe_4 SA. To maximize the number of Nb_2GeTe_4 layers, repetitive stripping was done by using a blue tape. The material on the tape was pressed by the optical fiber cabler and transferred to it after being stripped several times. A terminated fiber adapter was then used to link the patch cable to another equally clean one. The material created SA must completely cover the core in order to ensure that all of the light beams in the optical fiber travel through the Nb_2GeTe_4. Consequently, a high-quality SA was obtained by numerous transfers and observations. Then the prepared Nb_2GeTe_4 SA was inserted into the ring cavity for passive Q-switching. The Nb_2GeTe_4 SA possesses a wide-band absorption in a range of 1000 nm to 1700 nm, and shows excellent saturated absorbent properties with a saturation intensity of ~ 0.41 MW/cm^2 as well as a modulation depth of $\sim 16.6\%$.[32] The combination of a 1-m un-pumped polarization-maintaining Yb-doped fiber (PM-YDF2) and a polarization-maintaining fiber Bragg grating (PM-FBG) was connected to the second-port of the PM-CIR to ensure the SLM operation. The central wavelength of the PM-FBG was about 1064 nm with a reflectivity of 90%, and the 3-dB bandwidth was as narrow as 0.08 nm. The light reflected in the cavity formed a dynamic grating with the incident signal light in the PM-YDF2, and selected the SLM laser. The remaining light, which is also the output laser, was extracted from the laser cavity through the PM-FBG.

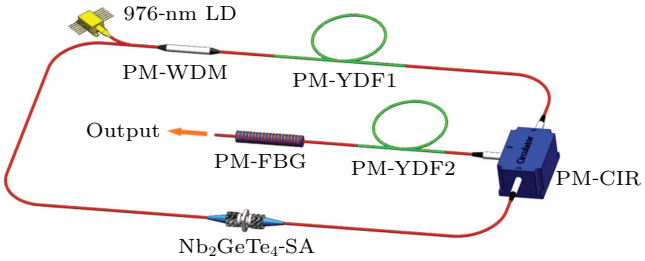


Fig. 1. Experimental setup of single-frequency linearly polarized Q-switched fiber laser based on Nb_2GeTe_4 SA.

3. Experimental results and discussion

The SLM operation is established by employing a section of PM-YDF and a PM-FBG. The PM-FBG enables 10% of the signal light output without reflection, while it reflects 90% of the signal light to the cavity. The reflected light together with the incident signal light generates standing wave interference in the PM-YDF2 and causes periodic spatial hole burning (SHB), resulting in refractive index changing periodically along the longitudinal direction of the PM-YDF2. Thus, the dynamic grating with ultra-narrow bandwidth is formed to achieve an SLM laser output.

The frequency interval between two adjacent longitudinal modes of the resonant cavity is calculated to be about 29 MHz from $\Delta\nu = c/(n_{\text{eff}}L)$, where $c = 3\times10^8$ m/s is the speed of light in vacuum, $n_{\text{eff}} = 1.47$ is the refractive index of the fiber, and $L = 7$ m is the length of laser cavity. The bandwidth of PM-FBG is 0.08 nm ($\Delta\lambda = 0.08$ nm), corresponding to a linewidth of 21 GHz ($\Delta\nu = 21$ GHz). The linewidth of PM-FBG is much longer than the frequency interval, so the resonant cavity allows MLM oscillation.

The PM-YDF2 together with PM-FBG is used as an ultra-narrow bandwidth filter in the experiment to perform the frequency selection operation. According to the coupled-mode theory, the expression for equivalent bandwidth of the dynamic grating is given as follows:[33,34]

$$\Delta\nu(\lambda,\Delta n) \approx \frac{\Delta n c\delta}{\lambda^2 n_{\text{eff}}^2}\sqrt{\Delta n^2 + \frac{\lambda^2}{L_{\text{YDF}}^2}}. \tag{1}$$

Here, $\Delta n < 2 \times 10^{-7}$ is the modulation amplitude of refractive index, $\delta = 1$ m is the dimension compensation parameter of mode coupling, and L_{YDF} is the length of PM-YDF2. In our experiment, λ, n_{eff}, and L_{YDF} are 1064 nm, 1.47, and 1 m, respectively. The theoretical bandwidth of the dynamic grating $\Delta\nu$ is about 27 MHz calculated from Eq. (1), which is smaller than the frequency interval of 29 MHz, so the SLM operation can be realized.

The characteristics of the output laser are measured. The following analysis focuses on the frequency–domain characteristics, time–domain performance, and power of the output laser.

The single-frequency pulsed laser is achieved in a pump power range of 240 mW–350 mW. The frequency–domain characteristics of the laser measured by Fabry–Perot interferometry with a free spectral range (FSR) of 4 GHz are given in Fig. 2(a), showing that the laser operates in the SLM regime. Figure 2(b) displays the typical frequency–domain characteristics of the single-frequency pulsed laser. The red line represents the experimental data, and the spectral line exhibits a discrete spike sequence resulting from the pulsed laser. The blue line is its fitted curve, and the laser linewidth of the laser is 28.4 MHz. Figure 2(c) gives the optical spectrum at the pump power of 300 mW, which is measured by an optical spectrum analyzer with a resolution of 0.02 nm. The central wavelength is 1064.6 nm, corresponding to the central wavelength of PM-FBG, and the signal-to-noise ratio (SNR) is greater than 47 dB. When the pump power increases to 360 mW, the laser changes from the SLM oscillation to the MLM oscillation, as can be seen in Fig. 2(d). This is attributed to the fact that as the pump power increases, the modulation depth of the index increases, resulting in a stronger dynamic grating. And the stronger grating reflects more light beams, thus less light is involved in the establishment of the dynamic grating, leading the dynamic grating to be weakened. The reflectivity decreases with the weakening of the dynamic grating, allowing more light to enter into the PM-YDF2 to participate in the establishment of the dynamic grating, so the dynamic grating is strengthened again. At the high pump power, it is in this dynamic cycle process, which greatly reduces the stability of grating and thus cannot trigger off a stable frequency selection mechanism. Consequently, the laser operates in the MLM regime.[35] The polarization characteristics of the laser are also measured by using an extinction ratio meter. Under different pump power, the polarization extinction ratio of the laser is about 30 dB.

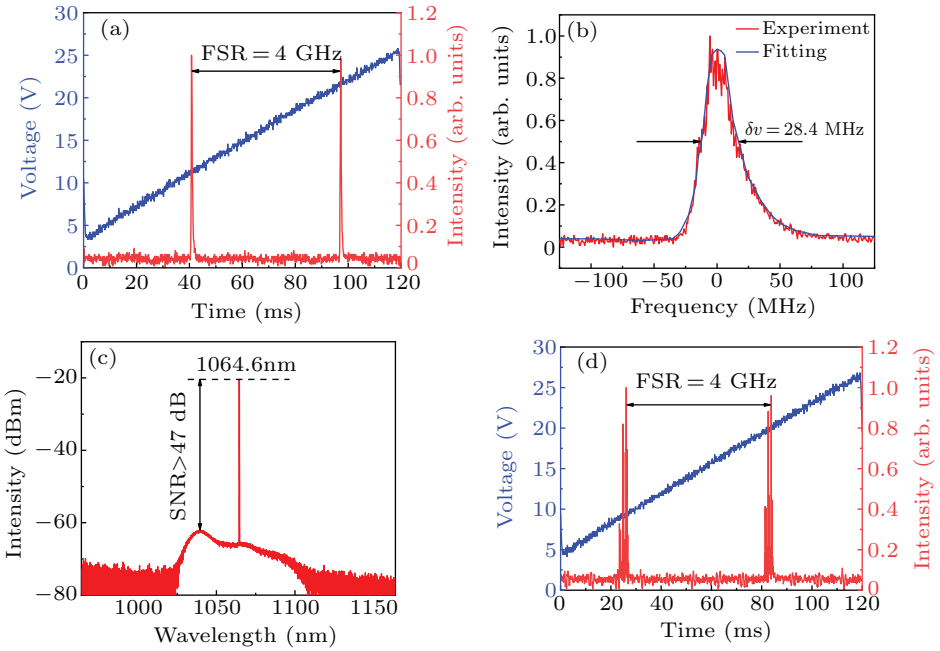


Fig. 2. Frequency–domain characteristics of SLM Q-switched laser: (a) longitudinal mode characteristics, (b) laser linewidth, (c) optical spectrum in a 200-nm span, and (d) MLM oscillation at pump power of 360 mW.

The obtaining of pulsed laser is based on the saturable absorption effect of the Nb_2GeTe_4 SA. The relationship between the absorption coefficient of the SA at the central frequency and the laser intensity is as follows:[36]

$$\alpha = \frac{\alpha_0}{1 + I/I_{\mathrm{s}}}. \tag{2}$$

Here, α is the absorption coefficient of the small signal light at the central frequency; I and I_{s} are the incident light intensity and saturated light intensity at the central frequency, respectively. It can be seen from Eq. (2) that the absorption coefficient decreases with the incident light intensity increasing. And when the light is extremely strong, the absorption coefficient is nearly zero and almost all of the incident light beams are transmitted. The process of generating pulse trains by using SA for passive Q-switching is as follows. At the beginning

of the pump, the laser cannot be initiated, which is because the large absorption coefficient of the SA results in the large loss in the ring cavity. With the accumulation of the population inversion, the amplified spontaneous emission gradually increases. The absorption coefficient decreases significantly when the light intensity is comparable to the saturation light intensity, and the laser starts to oscillate. As the laser intensity increases, the absorption coefficient continues to decline, which in turn leads the laser intensity to increase more rapidly, forming a positive feedback process in the laser and establishing a high-intensity pulsed laser.[36]

The stable pulse trains in a pump power range of 240 mW–350 mW are obtained. Interestingly, the time–domain performance of the laser is optically bistable in a pump power range of 240 mW–290 mW. No pulse trains are observed when the pump power increases from 240 mW to 290 mW. Further increasing the pump power to 300 mW, it can be seen that there is an output of pulse trains. Then the pump power decreases gradually, and only when the pump power decreases to 230 mW, will there be no output of pulse trains. By repeating the process, the phenomenon can be reproduced, indicating that the time–domain performance of the laser is optically bistable in a pump power range of 240 mW–290 mW. That is, in the optically bistable range of 240 mW–290 mW), no pulse trains are obtained when the pump power increases, while there is an output of pulse trains in the process of reducing the pump power as shown in Fig. 3. Moreover, when the pump power decreases to 230 mW, no pulse trains are observed. The reason is that the pump power is too small to reach the threshold of the SA, thus the cavity loss is so large that the laser cannot initiate oscillation. When further increasing the pump power over 360 mW, it can be observed that the pulse trains become unstable with strong amplitude fluctuations and even disappear, and the corresponding frequency–domain characteristics behaves as the MLM state. The phenomenon may be associated with the over-bleaching of the Nb_2GeTe_4 SA at high pump power.[25]

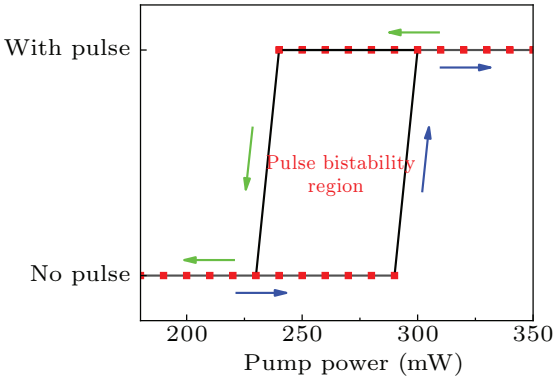


Fig. 3. Evolution of time–domain performance of laser with pump power.

To further clarify the time–domain performance of the SLM pulsed laser, the typical pulse trains at different pump powers, as shown in Fig. 4(a), are measured by using a digital oscilloscope and a photoelectric detector. It is illustrated in Fig. 4(a) that the repetition rate gradually increases with pump power increasing. The pulse width, repetition rate, and average power each as a function of the pump power are also measured. The pulse width decreases from 1.84 μs to 1.36 μs when the pump power increases from 240 mW to 350 mW as displayed in Fig. 4(b). It can be illustrated by the following explanation. As the pump power increases, $\Delta n_i/\Delta n_t$ becomes larger, where Δn_i is the initial population inversion and Δn_t is the critical population inversion. And a larger $\Delta n_i/\Delta n_t$ means a larger gain coefficient in the cavity, which leads the number of photons in the cavity to increase faster, and the population inversion to decay more rapidly. Thus, the pulse build-up and extinguishing time becomes shorter, that is, the pulse width becomes narrower.[36] As can be seen in Fig. 4(b), when the pump power varies from 240 mW to 350 mW, the repetition rate almost linearly increases from 28.3 kHz to 95.9 kHz. This is due to the fact that the power density in the cavity increases continuously as the pump power increases, so the time to reach saturation absorption turns shorter, corresponding to a higher repetition rate. Figure 4(b) shows that the average power of the laser grows linearly with the pump power increasing. It is indicated that as the pump power increases, the slope efficiency of average power remains nearly the same value, *i.e.*, 2.6%.

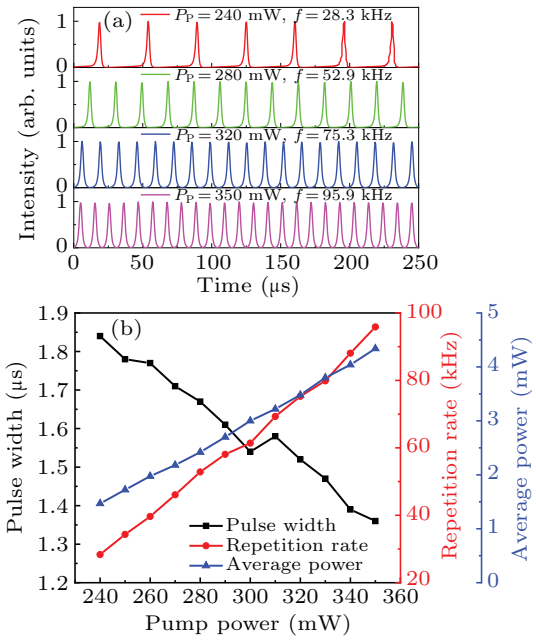


Fig. 4. (a) Variations of pulse trains with time for different pump powers, and (b) variation of pulse width, repetition rate, and average power with pump powers.

When the pump power values increase to 240 mW, 270 mW, 290 mW, 310 mW, 330 mW, and 350 mW, the single-pulse energy values are 51.8 nJ, 47.3 nJ, 46.5 nJ, 46.5 nJ, 47.6 nJ, and 45.3 nJ, respectively, and the corresponding peak power values are 33.5 mW, 36.9 mW, 38.5 mW, 36.3 mW,

36.3 mW, and 32.8 mW, respectively. It can be observed that the single-pulse energy and the peak power fluctuate up and down with the increase of the pump power. This phenomenon may be attributed to the combined effect of two aspects. On the one hand, the increase of the pump power leads the total energy of all pulses to increase within a certain time. And on the other hand, the repetition rate increases with pump power increasing, and the number of pulses also increases within a certain time, resulting in the decline of single-pulse energy. The single-pulse energy or peak power increases due to the fact that the effect of raising the total pulse energy is greater than that of increasing the repetition rate caused by increasing the pump power; and vice versa.

Finally, the fiber laser is continuously observed for 7 h under the pump power of 340 mW. Figure 5 shows that the spectrum is quite stable, and the output power fluctuates slightly around 4 mW.

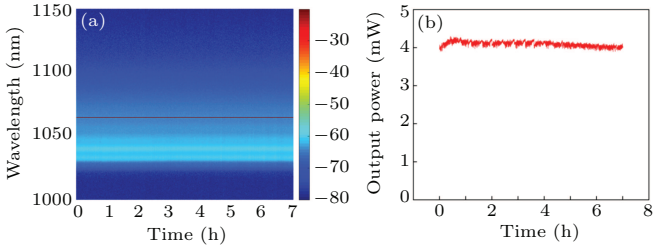


Fig. 5. Output laser properties within 7 h under pump power of 340 mW, showing (a) stability of spectrum and (b) stability of output power.

4. Conclusions

In this work, a single-frequency linearly polarized *Q*-switched fiber laser based on an Nb_2GeTe_4 SA is proposed. The pulse trains are achieved by using the saturable absorption effect of the Nb_2GeTe_4 SA. The PM-YDF2 combined with the PM-FBG forms a dynamic grating, which acts as an ultra-narrow bandwidth filter to achieve a stable SLM laser output. The SLM pulsed laser at 1064.6 nm is obtained, and it possesses a repetition rate in a range of 28.3 kHz–95.9 kHz, a pulse width of 1.36 μs–1.84 μs, a linewidth of 28.4 MHz, a polarization extinction ratio of about 30 dB, a maximum single-pulse energy value of 51.8 nJ, and a maximum peak power value of 39 mW. Compared with the MLM pulsed laser, the SLM pulsed laser possesses high stability and low noise. This work is of significance in putting the SLM pulsed lasers into applications in lidar, coherent optical communication, and high-resolution optical sensing.

Acknowledgements

Project supported by the National Natural Science Foundation of China (Grant No. 62275272) and the Training Program for Excellent Young Innovators of Changsha, China (Grant No. KQ2206003).

References

[1] Wang Y, Huang W, Wang C, Guo J, Zhang F, Song Y, Ge Y, Wu L, Liu J, Li J and Zhang H 2019 *Laser Photon. Rev.* **13** 1800313
[2] Liu J, Chen Y, Li Y, Zhang H, Zheng S and Xu S 2018 *Photon. Res.* **6** 198
[3] Shakaty A A, Hmood J K, Mahdi B R, Mahdi R I and Al-Azzawi A A 2022 *Opt. Laser Technol.* **146** 107569
[4] Chen X, Xiao Q R, Jin G Y, Yan P and Gong M L 2014 *Chin. Phys. B* **23** 064218
[5] Chen Y, Zhang J, Zhu X, Liu J and Chen W 2019 *Opt. Eng.* **58** 086106
[6] Fu S, Shi W, Feng Y, Zhang L, Yang Z, Xu S, Zhu X, Norwood R A and Peyghambarian N 2017 *Journal of the Optical Society of America B* **34** A49
[7] Su R, Zhou P, Wang X, Zhang H and Xu X 2012 *Opt. Lett.* **37** 3978
[8] Tao Y, Zhang S, Jiang M, Li C, Zhou P and Jiang Z 2022 *Opt. Laser Technol.* **145** 107519
[9] Xiao H, Dong X L, Zhou P, Xu X J and Zhao G M 2012 *Chin. Phys. B* **21** 034207
[10] Fu S, Zhu X, Zong J, Li M, Chavez-Pirson A, Norwood R A and Peyghambarian N 2022 *Opt. Express* **30** 32600
[11] Xie Z, Shi C, Sheng Q, Fu S, Shi W and Yao J 2020 *Opt. Commun.* **461** 125262
[12] Kato S and Aoki T 2022 *Opt. Lett.* **47** 5000
[13] Feng Z, Yiyu G, Libin J and Qiao W 2021 *Laser Photon. Rev.* **15** 2100059
[14] Liu S, Li G, Zhu F, Huang H, Lu J, Qu J, Li L and Wen Q 2022 *Adv. Funct. Mater.* **32** 2112252
[15] Yeh C H, You W Y, Chen J R, Chow C W and Lin W P 2020 *IEEE Photon. J.* **12** 1
[16] Fang S, Zhou B, Guan Z, Yang C, Zhao Q, Lin W, Feng Z and Xu S 2021 *Appl. Opt.* **60** 10684
[17] Zhang Y, Wang S, Lin W, Mo S, Zhao Q, Yang C, Feng Z, Deng H, Peng M, Yang Z and Xu S 2017 *Appl. Phys. Express* **10** 052502
[18] Zhang Y, Yang C, Feng Z, Deng H, Peng M, Yang Z and Xu S 2016 *Opt. Express* **24** 16149
[19] Li W, Liu H, Zhang J, Yao B, Feng S, Wei L and Mao Q 2017 *IEEE Photon. J.* **9** 1
[20] Wang W, Qi H, Song Z, Guo J, Ni J, Wang C and Peng G 2020 *Opt. Commun.* **467** 125747
[21] Zhao Q, Wu Z, Zhang Z, Lin W, Li C, Guan X, Tan T, Yang C, Cheng H and Gan J 2018 *Opt. Express* **26** 17000
[22] Peng Y, Zhang A, Pan H, Liu Z, Guo T, Zhen C, Li P and Du P 2022 *Optics and Laser Technology* **150** 108001
[23] Ahmad H, Hidayah Abdul Kahar N, Yusoff N, Zharif Samion M, Aisyah Reduan S, Faizal Ismail M, Bayang L, Wang Y, Wang S and Sahu J K 2022 *Opt. Fiber Technol.* **69** 102851
[24] Sun S, Yang F, Sui Z, Zhu M, Chen S, Wang Y, Hong Z, Zhang W, Fu S, Chen X, Wang G and Zhang H 2022 *J. Lumin.* **250** 119064
[25] Li W, Zou J, Huang Y, Wang K, Du T, Jiang S and Luo Z 2018 *Photon. Res.* **6** C29
[26] Ahmad H, Mansor N H, Reduan S A, Samion M Z, Yusoff N and Bayang L 2022 *Optics and Laser Technology* **156** 108510
[27] Wang Y, Zhu X, Sheng C, Li L, Chen Q, Zong J, Wiersma K, Chavez-Pirson A, Norwood R A and Peyghambarian N 2017 *IEEE Photon. Technol. Lett.* **29** 743
[28] Lai X, Li J, Luo H, Zhu C, Hai Y, Shi Y, Gao Y and Liu Y 2018 *Laser Phys. Lett.* **15** 085109
[29] Wang Y, Wang J and Wen Q 2021 *Nanomaterials (Basel)* **11** 720
[30] Gupta P K, Singh C P, Mukhopadhyay P K and Bindra K S 2022 *J. Opt.* **24** 054012
[31] Kong L, Chu H, Li N, Pan H, Zhao S and Li D 2022 *Chin. Opt. Lett.* **20** 051601
[32] Dai Y, Yu Q, Yang X, Guo K, Zhang Y, Zhang Y, Zhang J, Li J, Chen J, Deng H, Xian T, Wang X, Wu J and Zhang K 2022 *ACS Nano* **16** 4239
[33] Erdogan T 1997 *Journal of Lightwave Technology* **15** 1277
[34] Li Y, Huang L, Gao L, Lan T, Cao Y, Ikechukwu I P, Shi L, Liu Y, Li F and Zhu T 2018 *Opt. Express* **26** 26896
[35] Yin T, Song Y, Jiang X, Chen F and He S 2019 *Opt. Express* **27** 15794
[36] Zhou B K, Gao Y Z and Chen T R 2009 *The Principle of Laser*, 6th edn. (Beijing: National Defense Industry Press) p. 348 (in Chinese)